Clickable, Photodegradable Hydrogels to Dynamically Modulate Valvular Interstitial Cell Phenotype

*Chelsea M. Kirschner, Daniel L. Alge, Sarah T. Gould, and Kristi S. Anseth**

Biophysical cues are widely recognized to influence cell phenotype. While this evidence was established using static substrates, there is growing interest in creating stimulus-responsive biomaterials that better recapitulate the dynamic extracellular matrix. Here, a clickable, photodegradable hydrogel substrate that allows the user to precisely control substrate elasticity and topography in situ is presented. The hydrogels are synthesized by reacting an 8-arm poly(ethylene glycol) alkyne with an azide-functionalized photodegradable crosslinker. The utility of this platform by exploiting its photoresponsive properties to modulate the phenotype of porcine aortic valvular interstitial cells (VICs) is demonstrated. First, VIC phenotype is monitored, in response to initial substratum modulus and static topographic cues. Higher modulus ($E \approx 15$ kPa) substrates induce higher levels of activation (≈70% myofibroblasts) versus soft ($E \approx 3$ kPa) substrates (≈20% myofibroblasts). Microtopographies that induce VIC alignment and elongation on low modulus substrates also stimulate activation. Finally, VIC phenotype is monitored in response to sequential in situ manipulations. The results illustrate that VIC activation on stiff surfaces (≈70% myofibroblasts) can be partially reversed by reducing surface modulus (≈30% myofibroblats) and subsequently reactivated by anisotropic topographies (≈60% myofibroblasts). Such dynamic substrates afford unique opportunities to decipher the complex role of matrix cues on the plasticity of VIC activation.

1. Introduction

Physical properties of the cellular microenvironment, including substratum topography and modulus, play a significant role in regulating cellular function and fate.[1–3] In vivo cells receive biophysical cues through dynamic interactions with the extracellular matrix (ECM) and neighboring cells. Toward better understanding this dynamic exchange of information between cells and their ECM, there is a growing interest in developing materials for in vitro cell culture that can respond dynamically to user-defined stimuli.[4] In particular, hydrogels are often used as matrices to culture cells in two and three dimensions, and these water-swollen polymer networks are easily synthesized to span a range of tissue-like elasticities and/or to present various biological epitopes.[5] Beyond controlling initial hydrogel biochemical and biophysical properties, a class of photoresponsive hydrogels was developed that allows remotely triggered changes in hydrogel properties, in a spatiotemporal manner in the presence of cells.[6] These user-controlled dynamic responses have been used to engineer sophisticated cell culture scaffolds in 2D[7,8] and 3D,[9,10] drug delivery vehicles,[11] and actuators in microfluidic devices[12] and biosensors.[13]

Photodegradation of nitrobenzyl ether-containing poly(ethylene glycol) (PEG)-diacrylate (PEGDA) hydrogels, in particular, has been employed to modulate the physical properties of hydrogels including the material modulus[7] and the presentation of topographic features[14] to cell populations. Recently, two studies exploited this photolabile hydrogel system to investigate the influence of dynamically changing substratum elasticity, in the presence of valvular interstitial cells (VICs) isolated from porcine heart valves, on the fibroblast-to-myofibroblast transition.[15,16] VICs, like other fibroblasts, are responsible for maintaining tissue homeostasis[17,18] and, hence, play an important role in heart valve repair. In response to injury, VICs activate from a quiescent fibroblast phenotype to a myofibroblast,[19–22] a cell with both fibroblast and muscle cell characteristics,[23] elevated secretory properties,[19–22] and increased contractility.[21] A hallmark of VIC myofibroblasts is expression of α-smooth muscle actin (α-SMA) stress fibers.[24] The contractile activity of VIC myofibroblasts is beneficial for tissue remodeling but can be detrimental for tissue function[19,25]; therefore, under normal wound-healing conditions, it is terminated when the tissue is repaired.[18] The pathological persistence of myofibroblasts can lead to fibrosis characterized by excess matrix deposition and tissue stiffening.[19,26,27] In both studies, stimulus-responsive hydrogels facilitated controlled in vitro experiments to investigate the signals that regulate myofibroblast deactivation. VICs

Dr. C. M. Kirschner, Dr. D. L. Alge,
Dr. S. T. Gould, Prof. K. S. Anseth
Department of Chemical and
Biological Engineering and the BioFrontiers Institute
University of Colorado, 596 UCB, Boulder
CO 80303–0596, USA
E-mail: kristi.anseth@colorado.edu
Dr. D. L. Alge, Prof. K. S. Anseth
The Howard Hughes Medical Institute
University of Colorado, 596 UCB, Boulder
CO 80303–1904, USA

DOI: 10.1002/adhm.201300288

seeded onto stiff hydrogels ($E \approx 32$ kPa) became activated, but this activation was reversible upon light-directed reduction of the substrate modulus to a more physiologic value ($E \approx 7$ kPa).[15,16] In short-term culture (<7 d), this deactivation was shown to occur through downregulation of the valvular myofibroblast phenotype instead of apoptosis.[15]

Beyond the influence of the stiffness of the cellular microenvironment, reports also suggest that cell morphology and alignment may also influence myofibroblast properties.[28] In one example, corneal epithelial cells were cultured on gratings ranging from 1400 to 4000 nm in width and results indicated that these nanoscale topographic cues modulated TGF-β-induced myofibroblast transformation and α-SMA stress fiber formation possibly through the upregulation of Smad7.[29] Likewise, in partially constrained tissue equivalents, differentiated, dermal myofibroblasts aligned parallel to free edges where different mechanical loading environments led to differences in local gene and protein expression.[30] Furthermore, interstitial fluid flow has been shown to induce collagen alignment and myofibroblast differentiation of VICs in vitro.[31] Although less is known about VIC response to substrate topographies, the development of intracellular contractile stress can be modulated by substrate topography and is a prerequisite for the expression of α-SMA stress fibers during the fibroblast to myofibroblast transition[17] and stress fiber formation increases after stimulation of actomyosin-mediated contractility.[24] For example, Ayala and Desai[32] demonstrated that fibroblasts cultured on "micropeg" topographies exhibited downregulation of α-SMA and that microtopographical control of gene expression was dependent on intracellular contractility. Aortic valve disease preferentially begins in the valve layer called the fibrosa,[33] where histological sections reveal that VICs are the most aligned and elongated.[34] Research also shows that increasing cellular aspect ratio through substrate patterning leads to an increase in actomyosin contractility in human mesenchymal stem cells.[35] Based on these findings, we hypothesized that VIC alignment and elongation induced by substratum topography could be used in conjunction with substratum modulus to direct changes in VIC phenotype.

To investigate the effects of dynamic changes in biophysical cues on VIC phenotype, we developed a clickable, photodegradable hydrogel system that allows the user to control both stiffness and the presentation of topographic cues in real time. More specifically, the hydrogels are formed via a copper-catalyzed step-growth polymerization between bi-functional poly(ethylene glycol) (PEG) azide and octa-functional PEG-alkyne macromers, where photodegradability is achieved by incorporating a photolabile nitrobenzyl ether moiety into the PEG-azide. Here, the clickable, photodegradable hydrogel system provides predictable control of initial substratum elasticity over a large range of moduli (e.g., $E \approx 0.3$–15 kPa) and allows for spatiotemporal control over precise reductions in modulus and/or the presentation of engineered topographic cues to the cell population in situ. In this contribution, we characterize the initial mechanical properties of two hydrogel formulations designed to promote or suppress VIC activation. Then, we regulate the materials properties in situ by either i) bulk irradiation with 365 nm light to change the stiff activating substrates to soft microenvironments or ii) the erosion of micron-sized topographic features into the hydrogel surface using photolithographic patterning techniques to control VIC alignment. First, VIC activation is characterized by immunocytochemical staining for α-SMA stress fiber formation in response to both initial substrate modulus and anisotropy induced by contact guidance along topographic features. Subsequently, experiments are designed to demonstrate both the utility of sequential changes in the material properties and the plasticity of the VIC phenotype by seeding VICs onto stiff surfaces and monitoring phenotype, as the substrates are first softened and then patterned. Collectively, this cell culture platform will allow users to further characterize VIC function and pathobiology related to dynamic changes in substrate stiffness and cellular morphology and may lead to improved in vitro models for studying valve fibrosis.

2. Results and Discussion

2.1. Synthesis of Clickable, Photodegradable Hydrogels

A photodegradable cross-linker was synthesized by conjugating an azide-functionalized nitrobenzyl ether moiety to both ends of a linear poly(ethylene glycol) (PEG)-*bis*-amine ($M_n \approx 3400$ g mol^{-1}). This cross-linker was reacted via a copper-catalyzed click reaction with an 8-arm PEG-alkyne (PEG-yne) of two different molecular weights (i.e., $M_n = 10\,000$ g mol^{-1} or $M_n = 40\,000$ g mol^{-1}) to create hydrogels with a range of moduli (**Figure 1**a), similar to what has been described previously.[36,37] An azide-functionalized arginine-glycine-aspartic acid (RGD) peptide was included in the hydrogel formulation at 2×10^{-3} M to promote integrin-mediated VIC adhesion.[38,39]

To demonstrate the ability to precisely tune the initial modulus in the hydrogel, we formulated a series of macromer solutions using the two 8-arm PEG-yne macromers with different molecular weights and by varying the total macromer weight percent (e.g., 5, 10, and 15 wt%) while keeping the ratio of azide to alkyne moieties equal. Rheological measurements were performed to quantify the shear elastic modulus (G) of each construct, which was then converted to a Young's modulus (E) using rubber elasticity theory assuming a Poisson's ratio (ν) of 0.5 for bulk measurements of an elastic PEG-hydrogel network.[16] The Young's modulus for each construct scaled directly with total weight percent of macromer in solution during gel formation and indirectly with PEG-yne molecular weight, as expected (Figure 1b). The modulus conversion was performed because it was previously reported that substrates with a Young's modulus above 15 kPa activate (≈50% myofibroblasts) VICs to their myofibroblast phenotype, whereas substrates below this value (e.g., $E = 7$ kPa) do not (≈5% myofibroblasts).[16]

With this threshold in mind, we selected two hydrogel formulations for cell culture studies, namely the 10K PEG-yne macromer at 15 wt% as a "stiff" and activating formulation ($E \approx 15$ kPa) and the 40K PEG-yne macromer at 10 wt% as a "soft" and inactivating formulation ($E \approx 3$ kPa) (Figure 1b).[38,40] More specifically, the final gel-forming monomer solutions contained: 1) 5.99 wt% 8-arm PEG-alkyne ($M_n = 10\,000$ g mol^{-1}, [yne] = 46×10^{-3} M), 9.61 wt% azide-functionalized photodegradable cross-linker ([azide] = 44×10^{-3} M), 2×10^{-3} M azide-RGD,

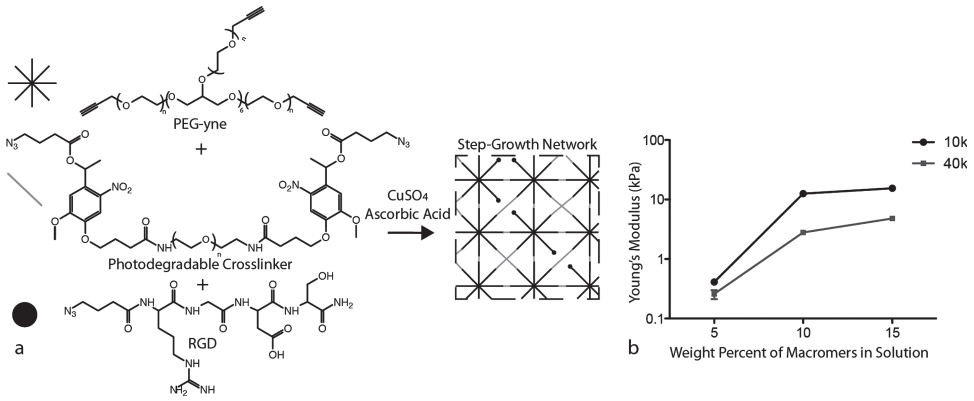

Figure 1. Hydrogel composition, network structure, and substrate modulus. a) The clickable, photolabile hydrogels were synthesized by reacting an 8-arm PEG-yne with an azide-functionalized photodegradable cross-linker via a copper-catalyzed click reaction, forming a step-growth network functionalized with RGD to promote cell adhesion. b) Bulk rheology of swollen hydrogel samples demonstrates that these materials can be altered through the PEG molecular weight and/or initial macromolecular solution concentration to create hydrogels that both have a modulus high enough to induce VIC activation ($E \approx 15$ kPa) and low enough to maintain a quiescent fibroblast phenotype ($E \approx 3$ kPa). Error bars: 95% confidence intervals.

0.1 wt% copper sulfate pentahydrate and 1 wt% sodium ascorbate in PBS for stiff hydrogels or 2) 7.1 wt% 8-arm PEG-alkyne (M_n = 40 000 g mol^{-1}, [yne] = 14×10^{-3} M), 2.5 wt% azide-functionalized photodegradable cross-linker ([azide] = 12×10^{-3} M), 2×10^{-3} M azide-RGD, 0.1 wt% copper sulfate pentahydrate and 1 wt% sodium ascorbate in PBS for soft hydrogels.

2.2. Manipulation of Hydrogel Properties Through Spatiotemporally Controlled Photodegradation

This hydrogel design was selected to allow spatiotemporal control of surface topographies through mass loss, as photodegradable step-growth networks display considerably faster erosion rates than chain-growth-polymerized networks.[41] Yet tunable bulk modulus reduction is also possible in these photodegradable hydrogels, as the octa-functional PEG-yne macromer leads to high network connectivity and a relatively wide range of modulus softening before reverse gelation is reached. The critical fraction of photocleavable bonds that must be broken to reach reverse gelation in these hydrogels, P_{rg}, which was previously defined by Tibbitt et al.,[31] is approximately 0.6. In contrast, if a tetra-functional PEG-yne were used, P_{rg} would be ≈0.4, meaning that the selection of octa-functional precursors allows for much longer irradiation times and a wider dynamic modulus range.

In these clickable, photodegradable hydrogels, the kinetics of photodegradation are dictated by the quantum yield of the photolabile nitrobenzyl ether moiety, the irradiation intensity, and the wavelength of light. To verify that the hydrogels follow the expected photocleavage kinetics and are consistent with prior reports on nitrobenzyl ether-containing hydrogels,[7,41,42] the photodegradation kinetics of each formulation where characterized by in situ rheology. Briefly, optically thin films (≈10 μm) were polymerized in situ between two parallel plates on a rheometer and exposed to 365 nm light at 2.5, 5, or 10 mW cm^{-2} until reverse gelation was reached. In general, the modulus of the gels decreased with irradiation time in a dose-dependent manner (**Figure 2**a,b). By fitting the curves to an exponential model (Figure S1, Supporting Information), effective rate constants for the photodegradation at 365 nm, k_{eff}, were calculated to be 2.9 ± 0. 4 and 3.9 ± 0.5 × 10^{-3} cm^2 mJ^{-1} for the stiff and soft formulations, respectively ($p < 0.05$; Table S1, Supporting Information). Although slightly different from each other, these numbers are comparable to what has previously been reported for nitrobenzyl ether-containing hydrogels.[7,9,41–44] Part of the difference between the two formulations might be attributed to slight differences in light attenuation, as the higher concentration of photodegradable PEG-azide macromer in the stiff formulation (ε_{365} = 2875 M^{-1} cm^{-1}; Figure S2, Supporting Information) resulted in an ≈3.5-fold increase in light attenuation through the thickness of the gel (Table S2, Supporting Information). In addition, slight differences in non-idealities in the hydrogel network resulting from chain entanglement may have contributed to the observed differences in the hydrogel photodegradation kinetics.

Importantly, from a quantitative understanding of hydrogel photodegradation, precise and predictable user-directed manipulations of hydrogel modulus are possible. To demonstrate this and also to develop a protocol for dynamic modulation of VIC phenotype, we explored softening of the stiff hydrogel formulation. More specifically, we sought to show that the modulus of the stiff formulation, which was chosen to be above the threshold for VIC activation to the myofibroblast phenotype, could be reduced to that of the soft, non-activating formulation. Briefly, using an irradiation dosage of 70 s at 9 mW cm^{-2} (i.e., 630 mJ cm^{-2}), the hydrogels could be softened to a modulus that was 16% of the initial value, almost precisely matching the soft formulation (Figure 2c).

In addition to softening, we were also interested in exploiting photodegradation of the hydrogel surface to create defined topographies at the cell-gel interface to study the influence of VIC alignment and elongation on myofibroblast activation.[33,34] In this case, gels were exposed to light doses that induced mass loss through a chrome-on-quartz photomask to generate channels microtopographies. Feature heights, which were measured

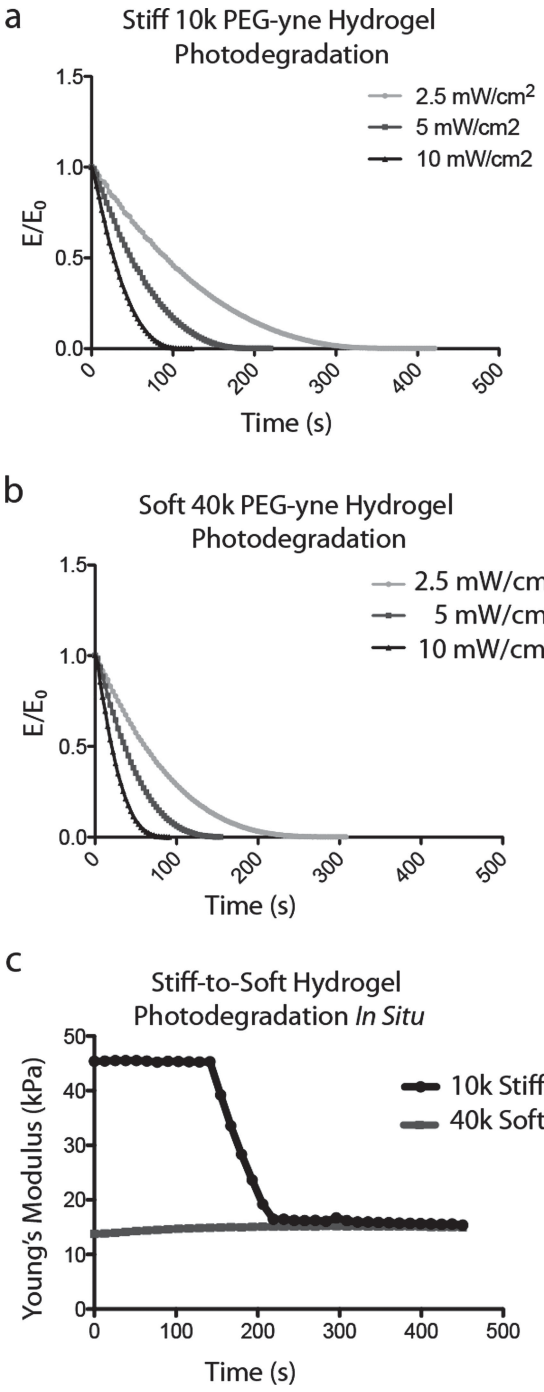

Figure 2. Photodegradation of hydrogel substrates. a,b) Representative photodegradation curves plotted as the ratio of the dynamic Young's modulus (E) to the initial Young's modulus (E_0) over time. Irradiation intensity controlled hydrogel degradation, i.e., higher intensity resulted in faster degradation. Photodegradation was also dependent on the original network structure. The 40K PEG-yne hydrogels degraded more quickly than the 10K PEG-yne hydrogels under the same irradiation conditions, most likely due to differences in light attenuation within the hydrogels as well as the presence of non-idealities in the network. c) Irradiation of 10 µm thin films of the Stiff 10K PEG-yne hydrogel for 70 s at 9 mW cm^{-2} during rheological testing resulted in a final modulus nearly identical to that of the Soft 40K PEG-yne hydrogel control, as predicted from the photodegradation kinetics.

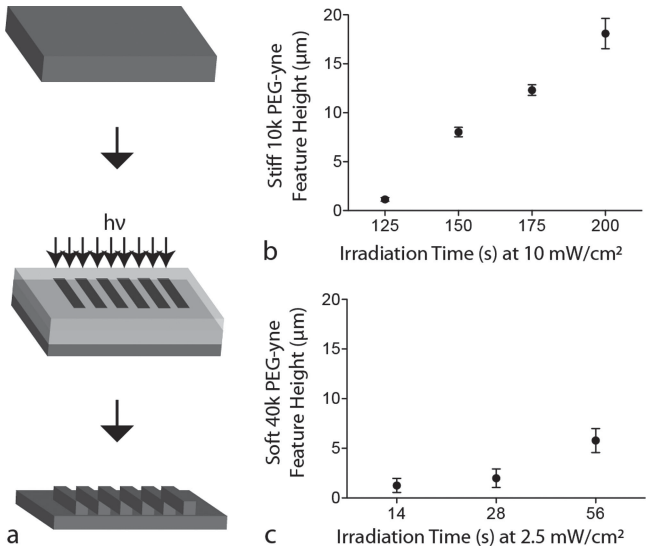

Figure 3. Fabrication of topographically modified hydrogel substrates. a) Smooth hydrogels were swollen to equilibrium and then irradiated with 365 nm, collimated light through a chrome-on-quartz photomask to produce topographically modified surfaces. b,c) Contact profilometry shows that feature height can be controlled by varying irradiation time at a fixed wavelength and intensity for stiff and soft hydrogel formulations, respectively Error bars: 95% confidence intervals.

by contact profilometry, scaled with UV exposure time and the stiff hydrogels required a higher light dosage to erode channels (**Figure 3**). Approximately, 1-µm deep channels were produced in the stiff hydrogels after 125 s of irradiation at 10 mW cm^{-2}. In contrast, even at 2.5 mW cm^{-2} light intensity, only 14 s of irradiation was needed to produce ≈1-µm deep channels in the soft gels. In addition to measuring the depth of erosion, fidelity of the pattern transfer in the x–w plane was quantified by imaging fluorescently labeled hydrogel constructs and analyzing the feature dimensions with ImageJ (Figure S3, Supporting Information). The average final dimensions of the topographical features in the gel were all within 4% of the originally defined mask feature sizes of 5 µm. All degradation experiments were performed under conditions that were previously shown to be cytocompatible[7] and based on our studies with VICs, the degradation products, short-PEG chains with carboxylic acid or ketone end-groups, were not expected to influence cell viability or function.[15,16]

2.3. Modulation of VIC Phenotype Using Static Biophysical Cues

To demonstrate the utility of this clickable, photodegradable hydrogel as a culture scaffold for studying and modulating VIC phenotype, we first confirmed VIC attachment and myofibroblast activation in response to the selected stiff ($E \approx 15$ kPa) and soft ($E \approx 3$ kPa) hydrogel formulations. VICs at passage 2 were seeded at 10 000 cells cm^{-2} on smooth hydrogels with and cultured for 3 d in low serum (1% FBS) medium to limit proliferation. Samples were then fixed and stained for the myofibroblast marker, α-SMA, along with ethidium homodimer to visualize nuclei. Activated myofibroblasts were identified as α-SMA-positive cells where the α-SMA was organized into stress fibers,

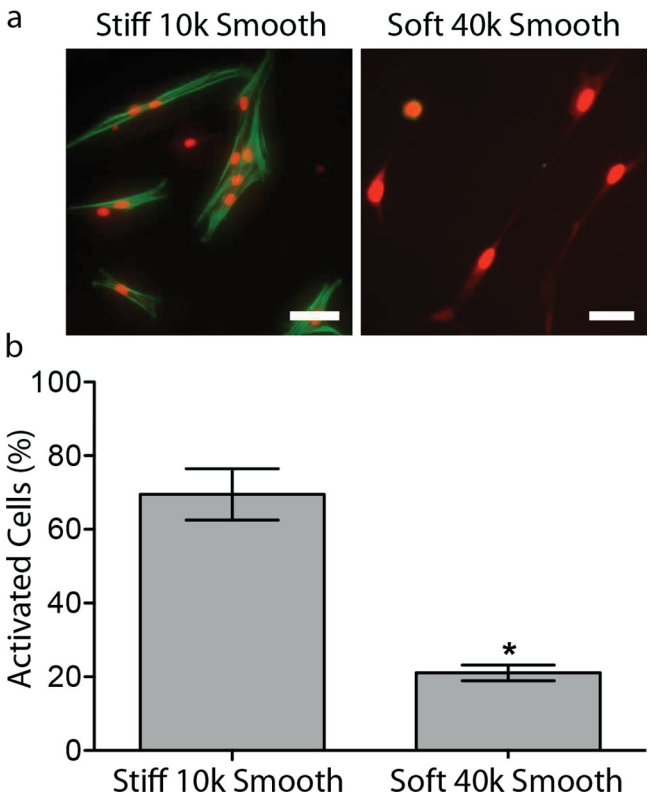

Figure 4. VIC activation in response to initial substrate elasticity. a) Representative images of immunocytochemical staining of α-SMA (green) and ethidium homodimer to visualize nuclei (red) in VICs on stiff (left) and soft (right) substrates. Activated myofibroblasts were identified as cells where α-SMA formed fibrils. Scale bars: 50 μm. b) The average percentage of activated cells on stiff and soft smooth substrates. Stiff substrates induced higher activation than soft. Error bars: 95% confidence intervals. Stars represent statistically significant differences (Marascuilo procedure, $\alpha = 0.05$).

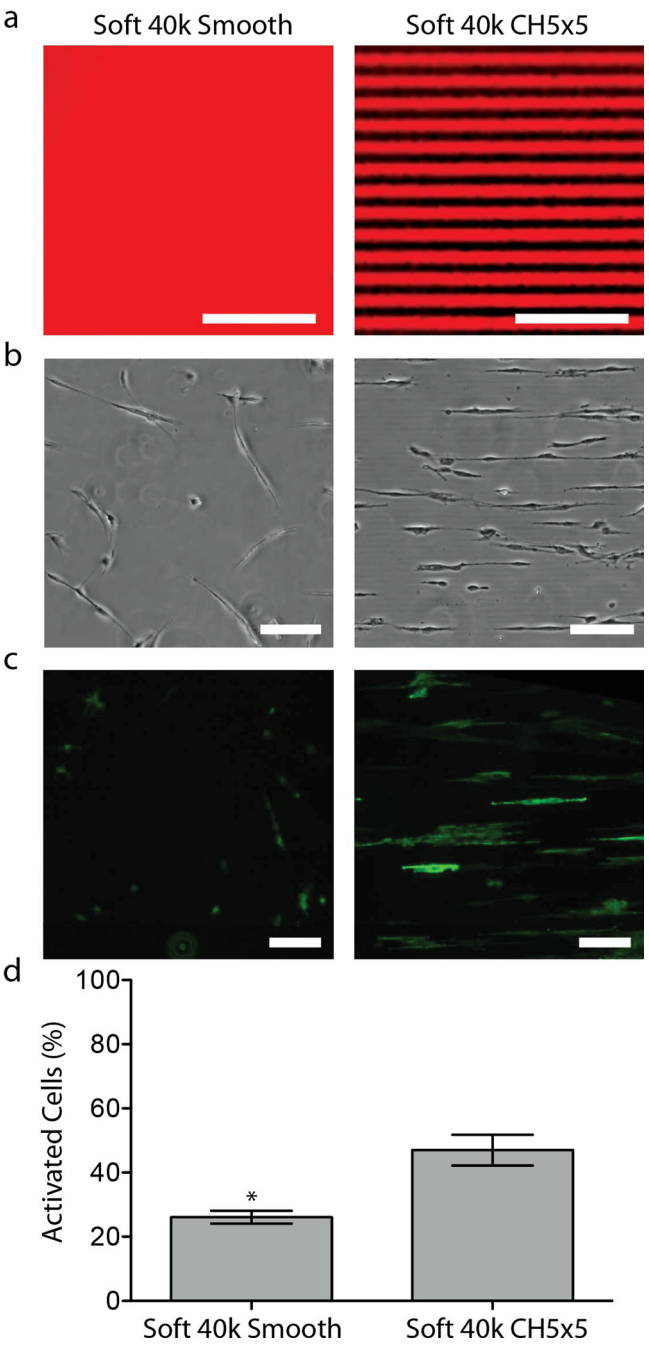

Figure 5. VIC response to topographically modified substrates. a) Soft hydrogel substrates covalently, fluorescently labeled with Alexa Fluor 555 Azide to visualize smooth and topographically modified, i.e., channels substrates. b) Brightfield, phase constrast images show VICs attach and spread on smooth hydrogels and exhibit contact guidance on channels. c) Immunocytochemical staining for α-SMA shows increased fibril formation and activation on the channels topographies. d) Quantification of α-SMA staining revealed approximately twofold increase in activation on channels microtopographies. Scale bars: 50 μm.

and VIC activation was quantified by counting the numbers of activated and non-activated cells per in at least 10 random fields of view per sample with three replicates for each condition. The percentage of myofibroblasts was calculated as (number of α-SMA-stress fiber-positive cells/total number of cells) × 100%. In brief, stiff substrates induced a higher proportion of activated myofibroblasts (70% activated) versus soft substrates (21% activated), and confirmed previous observations related to VIC activation using different types of PEG hydrogel systems (**Figure 4**).[15,16] Given the ability to induce activation of VICs or promote the maintenance of the quiescent phenotype by selection of the substrate elasticity, we next sought to examine the response of VICs to topographical cues that might induce alignment, on these same hydrogel formulations.

Channel microtopographies, 5 μm wide with 5 μm spacings, have been previously shown to induce high levels of alignment and elongation based on orientation and cellular aspect ratio (AR ~7) measurements in human mesenchymal stem cells.[14] For this reason, similar channel topographies were replicated in both the stiff and soft hydrogel substrates (**Figure 5**a). For all VIC experiments, irradiation conditions were selected that resulted in feature heights of ≈1 μm in each hydrogel system to allow for directed cell spreading and alignment without the physical constraint that might be induced by features that are much deeper than the cell height. On day 3, samples were again fixed and stained for α-SMA and ethidium homodimer

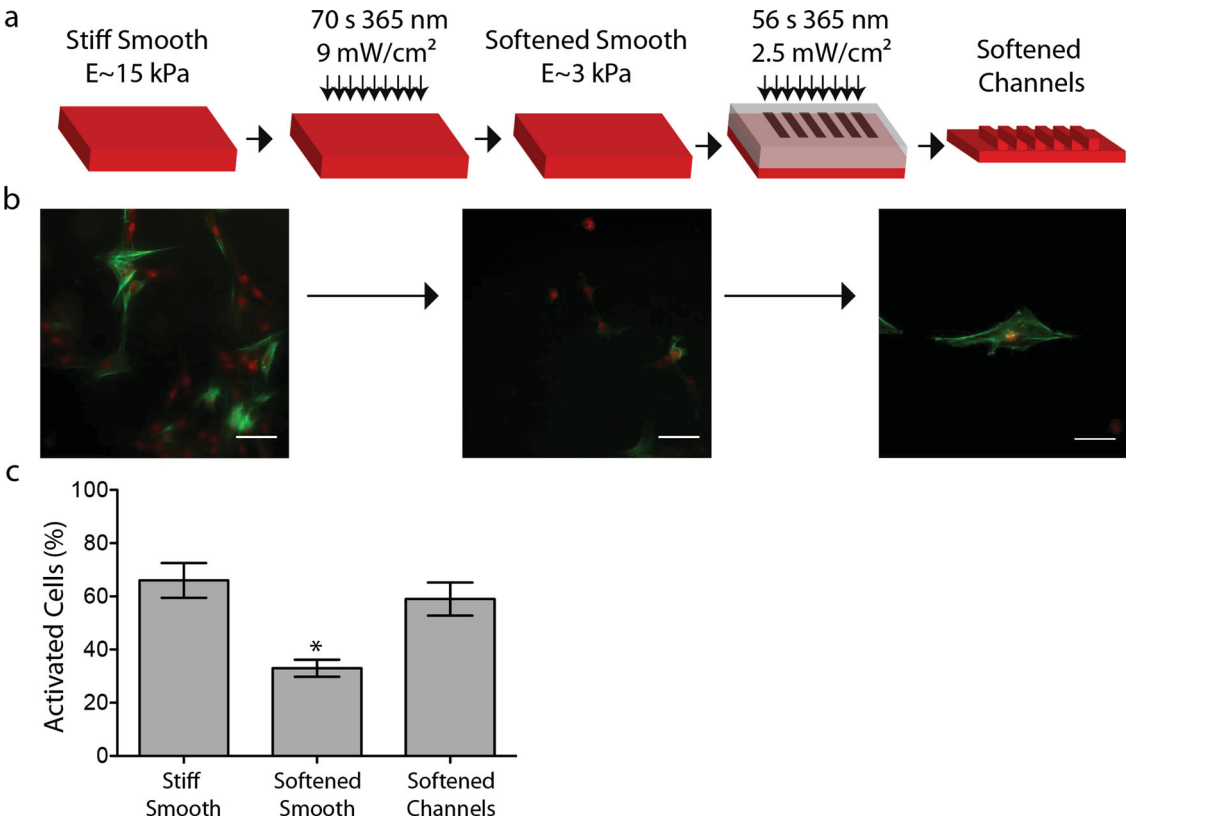

Figure 6. VIC response to dynamic physical cues. a) A schematic of the process employed to expose a VIC population to a series of physical cues: stiff, soft, and soft channels-patterned substrates. VICs were initially seeded onto smooth, stiff substrates and cultured for 72 h in low serum media before the hydrogels were softened to E ~3 kPa via photodegradation (365 nm, 10 mW cm $^{-2}$, 70 s). After softening in situ, the same VIC-laden gels were cultured for an additional 48 h in low serum media before the softened hydrogels were patterned to create channels (365 nm, 2.5 mW cm $^{-2}$, 56 s). Cells were cultured for another 48 h after patterning before final analysis. b) VIC phenotype was monitored at all three stages of this process. Samples were fixed and stained for α-SMA along with ethidium homodimer to identify and quantify activated myofibroblasts. Scale bars: 50 μm. c) Culturing VICs on stiff substrates resulted in a relatively high proportion of activated myofibroblasts (66% activated), which was reduced after softening (33% activated). The subsequent presentation of channels on soft substrates induced cellular elongation and alignment and also recovered a higher percentage of myofibroblast activation in the same cell population (59%). Error bars: 95% confidence intervals. Stars represent statistically significant differences (Marascuilo procedure, $\alpha = 0.05$).

to identify and quantify the percentage of the VIC population that were activated to the myofibroblast phenotype. VICs attached and spread on the smooth hydrogels, while exhibiting contact guidance along the channels on the microtopographically modified substrates (Figure 5b). Interestingly, channels microtopographies created in the soft substrates increased activation approximately twofold versus smooth soft substrates (Figure 5c). This result may be attributed to the alignment of the VIC actin filaments, which could allow for increased VIC contractile force generation and subsequent addition of α-SMA stress fibers to the cytoskeleton. However, channels microtopographies created in the stiff substrates did not significantly influence activation (Figure S4, Supporting Information). We speculate that this observation is likely related to the fact that VICs are already highly activated on the stiff surfaces, so additional activation is limited through modification of cell morphology. Overall, these results demonstrate that VIC elongation and orientation along physical microtopographic cues can induce increased activation to the myofibroblast phenotype on otherwise non-activating surfaces.

2.4. Dynamic Modulation of VIC Phenotype

With these results in mind, we next sought to exploit the ability to dynamically change substrate modulus and topography in situ, to study how VICs might respond by activating or deactivating to changes in their microenvironment. VICs were cultured on the base stiff hydrogel formulation and then a series of changes in the microenvironment were introduced sequentially at experimenter-defined time points: initially stiff, softened, and then topographically patterned, all while monitoring changes in the VIC phenotype. A schematic of this process is depicted in **Figure 6**a. Samples were collected at each of the three stages of microenvrionmental changes, and each construct was stained for α-SMA along with ethidium homodimer to identify and quantify activated myofibroblasts (Figure 6b). In the initial state, VICs cultured on the stiff substrates became activated to myofibroblasts in 3 d (66% myofibroblasts), but this activation was partially reversed by softening the gel environment. Gels were softened to 3 kPa at day 3 and only 33% myofibroblasts were observed 2 d later. These results support findings in previous

literature,[15,16] but the third step extends these concepts to test if the deactivated VICs can be reactivated to myofibroblasts by the introduction of a second biophysical matrix cue. Here, the subsequent presentation of channels on the softened substrate induced cellular elongation and alignment and led to higher levels of myofibroblast activation (59%) in the same VIC population (Figure 6c).

Collectively, these results demonstrate the possibility of presenting a series of physical cues to a single-cell population both spatially and temporally. Here, we show that the VIC population continues to be responsive to activating cues (i.e., alignment) even after they have been deactivated, suggesting that the fibroblast-to-myofibroblast transition in VICs is relatively plastic. We find it interesting to compare these types of in vitro results to in vivo findings. For example, the fibrosa layer of the heart valve leaflet is prone to manifesting symptoms of disease first,[33] and the VICs in this layer after often elongated and aligned in a manner that correlates with collagen fiber organization.[34] Increased VIC activation to the myofibroblast phenotype with the anisotropic morphology of the cells in this region may also be related to increases intracellular contractility, a prerequisite for activation, and that could in turn lower the threshold for activation. Since the myofibroblast properties of VICs and the reversal of this activation are complex processes, but important for those interested in better understanding valve disease progression, it would be an interesting next step to present multiple biophysical cues in a complementary way such as increasing substrate modulus to mimic one aspect of fibrosis while cells are elongated. These types of experiments could allow researchers to better elucidate how elongated VICs in the fibrosa may respond differently to microenvironmental cues than those with a more isotropic morphology.

3. Conclusion

Here, a clickable, photodegradable cell culture scaffold was synthesized and characterized that allows for the modulation of biophysical cues in real time and in the presence of cultured cells. Experiments were conducted that demonstrate the ability to sequentially expose VICs to a series of physical cues in situ and revealed the ability to study the plasticity of VIC response to matrix cues, especially the fibroblast-to-myofibroblast transition. Controlled modulus changes allowed us to initially activate VICs to myofibroblasts (66%) on 15 kPa gels, but then partially reverse this activation (33%) by light-induced softening of the gel to 3 kPa. Finally, the patterning of channels into the same substrate led to reactivation in the same cell population (59% myofibroblasts). The ability to alter substrate stiffness and cellular morphology in situ, as we report here, could potentially be exploited to study how VICs respond to step or gradual changes in their extracellular microenvironment over time. Such experiments may prove useful for testing hypotheses about the role of microenvironment changes and their contribution to initial stages of valve disease progression. Of course, dynamic changes in cell-matrix interactions are broadly interesting across cells and tissue types, so this biomaterials approach may find broader application to researchers interested in biomechanical matrix signaling.

4. Experimental Section

Photodegradable PEG-Azide Synthesis: Nitrobenzyl azide was synthesized as previously described.[9] Complete synthetic details and spectroscopic characterization are in the Supporting Information. To obtain a nitrobenzyl azide-functionalized PEG macromer (PEG-diNBA), this molecule was conjugated to a PEG *bis*-amine using standard peptide-coupling chemistry. Briefly, 1 g (0.294 mmol) of PEG *bis*-amine (M_n = 3400 g mol^{-1}; Laysan Bio, Inc., Arab, AL, USA) was dissolved in minimal anhydrous *N,N*-dimethylformamide (DMF; Sigma–Aldrich, St. Louis, MO, USA) with 205 µL (1.47 mmol) of triethylamine (Sigma–Aldrich, St. Louis, MO, USA) and allowed to stir at room temperature for ≈15 min. In a separate vessel, 0.603 g (1.47 mmol) of nitrobenzyl azide was combined with 0.557 g (1.47 mmol) of O-benzotriazole-*N,N,N′,N′*-tetramethyl-uronium-hexafluorophosphate (HBTU; Chem-Impex International, Inc., Wood Dale, IL, USA), dissolved in minimal anhydrous DMF, and allowed to stir at room temperature for ≈5 min. The two vessels were then combined and the reaction was allowed to proceed overnight at room temperature. Crude product was subsequently obtained by precipitation in cold diethyl ether. Purification was achieved by dialysis against deionized water for 2 d. Lyophilization produced 1.005 g of PEG-diNBA as a light yellow solid (82% yield). Nitrobenzyl azide functionalization was estimated to be 95% by comparing integrations of the aromatic peaks from the nitrobenzyl azide moiety (7.54 and 7.09 ppm) to those of the PEG backbone (3.50 ppm). ^{1}H NMR (400 MHz, DMSO-d_6): δ = 7.93 ppm (t, J = 5.6 Hz, 2H; –CO–NH–), 7.54 ppm (s, 2H; Ar H), 7.09 ppm (s, 2H; Ar H), 6.20 ppm (q, J = 6.5 Hz, 2H; O–CH–), 4.04 ppm (t, J = 6.5 Hz, 4H; –CH_2–), 3.93 ppm (s, 6H; O–CH_3), 3.50 ppm (s; [CH_2CH_2O]$_n$), 3.39 ppm (t, J = 5.9 Hz, 4H; –CH_2–), 2.42 ppm (t, J = 7.3 Hz, 4H; –CH_2–), 2.24 ppm (t, J = 7.4 Hz, 4H; –CH_2–), 1.98 – 1.88 ppm (m, 4H; –CH_2–), 1.80 – 1.70 ppm (m, 4H; –CH_2–), 1.58 ppm (d, J = 6.5 Hz, 6H; –CH_3).

PEG-yne Synthesis: Octa-functional PEG-yne macromers were prepared from PEG-OH precursors of two molecular weights (M_n = 10 000 g mol^{-1} and 40 000 g mol^{-1}; JenKem Technology, Inc., Allen, TX, USA) using the method of van Dijk et al.[45] Both reactions were performed using 5 g of PEG starting material. The general reaction conditions were as follows: PEG was added to an argon-purged flask and dissolved in 75–100 mL of dry tetrahydrofuran (extra dry over molecular sieves; Acros Organics, NJ, USA). 2.5 equiv. of dry sodium hydride (Sigma–Aldrich, St. Louis, MO, USA) was added to the reaction portionwise while stirring vigorously. After ≈15 min, 2.5 equiv. of propargyl bromide (80 wt.% in toluene; Sigma–Aldrich, St. Louis, MO, USA) was added to the reaction via dropwise addition with a syringe. The reaction was allowed to proceed at room termperature overnight. After filtering off the sodium salts, the reaction mixture was concentrated by rotary evaporation and the crude PEG-yne products were precipitated from cold diethyl ether. After dialysis and lyophilization, the alkyne-functionalized PEG macromers were obtained as a white solid in ≈80% yield. Alkyne functionalization was estimated to be 90% by comparing integrations of the peaks from the propargyl group (4.20 and 2.43 ppm) to those of the PEG backbone (3.64 ppm). ^{1}H NMR (400 MHz, DMSO-d_6): δ = 4.20 ppm (d, J = 2.4 Hz, 16H; –O–CH_2–), 3.64 ppm (m; [CH_2CH_2O]$_n$), 2.43 ppm (t, J = 2.3 Hz, 8H; C≡CH).

N_3-RGD Synthesis: To promote cell attachment to the hydrogels, the fibronectin mimetic integrin-binding peptide RGD was synthesized using a standard Fmoc solid-phase peptide synthesis protocols. The synthesis was performed at the 0.25 mmol scale on an automated peptide synthesizer (Tribute Peptide Synthesizer; Protein Technologies, Tucson, AZ, USA) using Rink amide MBHA resin (Novabiochem, Darmstadt, Germany). During synthesis, Fmoc deprotection was achieved by treatment with 20% piperidine and 2% 2,8-diazobicyclo[5.4.0]undec-7-ene (Sigma–Aldrich, St. Louis, MO, USA) in *N*-methylpyrrolidone (NMP; Applied Biosystems, Grand Island, NY, USA). Amino acid coupling was performed in peptide synthesis grade DMF (Applied Biosystems, Grand Island, NY, USA) using four equiv. of protected amino acid (all from Chem-Impex International, Inc., Wood Dale, IL, USA), four equiv. of HBTU activator, and eight equiv. of 4-methylmorpholine

(Sigma–Aldrich, St. Louis, MO, USA). To minimize deletion sequences, capping was performed after each step using a solution of 5% acetic anhydride and 6% 2,6-lutidine (both from Sigma–Aldrich, St. Louis, MO, USA) in NMP. After the automated synthesis was complete, azide functionalization was achieved by solid-phase coupling of 4-azidobutyric acid (see the Supporting Information for synthetic details) to the N-terminus of the peptide. This coupling performed just as described for the amino acid couplings, and was verified using the ninhydrin test. Peptide cleavage and deprotection was achieved by treatment with trifluoroacetic acid/phenol/triisopropyl-silane/dH2O (90/5/2.5/2.5). The peptide was recovered by precipitation in cold diethyl ether, washed twice with cold diethyl ether, and then dried in a vacuum desiccator. The crude peptide was subsequently purified by reverse-phase HPLC (gradient = 5% acetonitrile in water for 3 min, 5%–20% acetonitrile over 7 min, 20–40 acetonitrile over 20 min; 20 mL min^{-1} flow rate; column = Waters XSelect CSH C18 OBD Prep Column, 130 Å, 5 μm, 30 mm × 150 mm) and lyophilized. The purified peptide was reconstituted in sterile PBS and stored at −70 °C until use. MALDI-TOF MS [M + H] calculated for $C_{19}H_{33}N_{11}O_8$ 544.5; found 543.8.

General Procedure for Hydrogel Polymerization: Clickable, photodegradable hydrogels were synthesized through a copper-catalyzed click reaction of an 8-arm PEG-alkyne (M_n = 10 000 g mol^{-1} or M_n = 40 000 g mol^{-1}) with an azide-functionalized photodegradable PEG cross-linker and an azide-functionalized RGD peptide to promote cell adhesion. The gel-forming monomer solution contained 5.99 wt% 8-arm PEG-alkyne (M_n = 10 000 g mol^{-1}), 9.61 wt% azide-functionalized photodegradable cross-linker, 2×10^{-3} M RGD, 0.1 wt% copper sulfate pentahydrate (Fisher) and 1 wt% sodium ascorbate (Sigma-Aldrich, St. Louis, MO, USA) in PBS for stiff hydrogels or 7.1 wt% 8-arm PEG-alkyne (M_n = 40 000 g mol^{-1}), 2.5 wt% azide-functionalized photodegradable cross-linker, 2×10^{-3} M RGD, 0.1 wt% copper sulfate pentahydrate (Fisher, Pittsburgh, PA, USA) and 1 wt% sodium ascorbate (Sigma Aldrich, St. Louis, MO, USA) in PBS for soft hydrogels. All components were dissolved in sterile PBS or sterile-filtered to avoid contamination in cell cultures. To visualize hydrogel substrates fluorescently, Alexa Fluor 555 Azide (Life Technologies, Grand Island, NY, USA) was incorporated into the hydrogel precursor solution (300×10^{-6} M). Each individual aliquot of the hydrogel precursors was initiated with copper sulfate and quickly pipetted into a mold made of two glass coverslips, one siliconized with Sigmacote (Sigma Aldrich, St. Louis, MO, USA) and the other treated with an azide-functionalized silane-coupling agent. Coverslips (18 mm, No. 2, Fisher) were silanted via liquid deposition of the silane, 0.5% 6-azidosulfonylhexyl-triethoxysilane (Gelest, Morrisville, PA, USA), in 95% ethanol/water solution for 3 min. Coverslips were then dried at 80 °C. Hydrogels were covalently attached to the glass coverslips via the silane-coupling agent during polymerization. Smooth hydrogel samples were soaked in 0.1 M ethylenediaminetetraacetic acid (EDTA) for 20 min at room temperature to chealate and remove any residual copper. The EDTA solution was aspirated and samples were subsequently rinsed three times with PBS. Hydrogels were then stored in ultra-low attachment 6-well plates (Corning, Corning, NY, USA) and swollen in PBS for at least 24 h before topographic modification or cell seeding.

Rheological Characterization: The rheological properties of swollen hydrogel films were measured as previously described.[46] Briefly, freestanding films of each hydrogel formulation were cast between two siliconized glass slides to produce discs (height: 1 mm; diameter: 7 mm), which were swollen to equilibrium for bulk rheological measurements. The storage and loss moduli (i.e., G' and G'') were quantified on a parallel plate rheometer (DHR-3, TA Instruments, New Castle Delaware, USA) equipped with an 8-mm plate. The hydrogels were subjected to an oscillatory shear at 1% strain through a dynamic angular frequency range of 0.1 to 100 rad s^{-1}.

Photodegradation Kinetics: The photodegradation kinetics of the soft and stiff hydrogel formulations were measured by in situ degradation on a rheometer, as previously described.[7] Briefly, the hydrogels were polymerized between 8 mm parallel plates on a Discovery DHR-3 rheometer (TA Instruments, New Castle Delaware, USA) equipped with an irradiation fixture connected to 365-nm UV light source (Omnicure, Mississauga, Ontario, Canada). In this experimental setup, gels were irradiated from the bottom through a fixed quartz plate. To minimize light attenuation through the hydrogel samples, a 10-μm gap size was used (see the Supporting Information for light attenuation calculations). After network evolution was complete (≈20 min), the shutter was opened on the UV light source, and the samples were irradiated until reverse gelation was reached. Three different light intensities were tested: 2.5, 5, and 10 mW cm^{-2}. Dynamic shear modulus measurements were recorded at 1 rad s^{-1} and 1% strain, which was within the linear viscoelastic regime for the hydrogels. The measurements when then converted to Young's modulus, and the kinetic constant for photodegradation was calculated by fitting E/E_0 to an exponential curve and using the following relationship:

$$\frac{E}{E_0} = e^{-kt} \tag{1}$$

Here, E is the instantaneous Young's modulus, E_0 is the initial Young's modulus, t is time, and k is the apparent rate of photodegradation. For photocleavage kinetics, k is defined as

$$k = \frac{\phi \varepsilon I_0}{N_A h \nu} = k_{eff} I_0 \tag{2}$$

where ϕ is the quantum yield of photodegradation, I_0 is the incident light intensity, N_A is Avogadro's number, h is Planck's constant, and ν is the frequency at the wavelength of irradiation. As all of the variables except I_0 can be considered as constants in our photodegradation experiments, an effective rate constant, k_{eff}, was defined by gathering all of the variables except I_0. This approach provides valuable information about how irradiation dosage can be used to tune the hydrogel modulus. Additional details and data for the curve fitting are provided in the Supporting Information.

Fabrication and Characterization of Topographically Modified Substrates: Photolithographic techniques were used as described previously[14] to topographically modify substrates. Briefly, smooth hydrogels attached to coverslips were swollen to equilibrium and placed into direct contact with the chrome side of a chrome-on-quartz photomask. Hydrogel surfaces were exposed to controlled irradiation by 365 nm, collimated light. Dosages were varied for each hydrogel formulation by adjusting UV intensity and exposure time to fabricate the desired feature heights. To create topographically modified surfaces for cell culture experiments, photolithography was performed inside a sterile biosafety cabinet. For dynamic experiments performed after seeding cells onto samples, photolithography was performed through a sterile mold made of a gasket (thickness: 20–50 μm, Artus Corporation, Englewood, NJ, USA) and a coverslip (25 mm, No. 1, Fisher, Pittsburgh, PA, USA).

ImageJ software was used to measure the dimensions of several channels in the x–y plane of fluorescent images for three replicates of each hydrogel formulation (Figure S3, Supporting Information). Feature heights were measured by contact profilometry (DekTak 6M Stylus Profiler, Veeco, Plainview, NY, USA).

VIC Culture: Aortic valve leaflets were excised from porcine hearts (Hormel Foods Corporation, Austin, MN, USA) within 24 h of sacrifice. Primary VICs were isolated from porcine aortic valve leaflets using a sequential collagenase digestion, as previously described.[47] The isolated cells were cultured in growth medium (Medium 199, 15% fetal bovine serum (FBS), 50 U mL^{-1} penicillin, 50×10^{-6} M mL^{-1} streptomycin, and 0.5 μg mL^{-1} amphotericin B) and expanded overnight. Passage 2 cells were seeded onto samples at 10 000 cells cm^{-2} in low serum (1% FBS) medium and cultured for 3–5 d. Medium was refreshed with low serum, differentiation medium after 3 d in culture for longer assays.

VIC Staining, Imaging, and Quantification: Immunocytochemical staining for α-SMA was used to identify activated myofibroblasts. All staining steps were performed at room temperature. Cells on hydrogels were fixed using a two-step process. First, half of the medium was removed from each well and replaced it with 4% paraformaldehyde

for 5 min. Then, this solution was replaced with 4% paraformaldehyde for an additional 10 min. The VICs were permeabilized in 0.2% Triton X-100 (Sigma Aldrich, St. Louis, MO, USA) for 10 min and samples were blocked with 5% bovine serum albumin (BSA, Sigma Aldrich, St. Louis, MO, USA) in PBS for 1 h. Mouse monoclonal anti-α-SMA antibody (Abcam, Cat# a b7817, Cambridge, MA, USA) was diluted at 1:200 in an immunofluorescence (IF) solution of 3% BSA with 0.1% Tween 20 in PBS. Cells were incubated with the primary antibody solution for 1 h. After washing with IF solution, samples were incubated with goat-anti-mouse IgG Alexa Fluor-488 secondary antibody (1:200 in IF solution, Sigma Aldrich, St. Louis, MO, USA) for 1 h. After washing with IF solution, the cells were incubated with ethidium homodimer (4×10^{-6} M, in PBS) for 30 min. Samples were subsequently washed with IF solution for 5 min and mounted using Prolong Gold Antifade reagent (Life Technologies, Grand Island, NY, USA) to preserve for imaging.

All microscopy was performed on an upright, epi-fluorescent microscope (Axio Examiner, Zeiss, Germany). To quantify activation on each sample, 10 random fields of view were imaged at 20× magnification. Activated myofibroblasts were counted as cells with α-SMA organized into stress fibers by counting merged images using the Cell Counter Plugin in ImageJ. The percentage of activated cells was calculated as (number of myofibroblasts/total number of cells) x 100%. All images from each replicate were counted and averaged to calculate the average percentage of activated cells. Statistical differences were determined using the Marascuilo procedure, $\alpha = 0.05$.

Supporting Information

Supporting Information is available from the Wiley Online Library or from the author.

Acknowledgements

The authors thank Prof. C. N. Bowman for use of the profilometer and K. M. Mabry for assistance isolating VICs. The authors acknowledge the National Institute of Arthritis and Musculoskeletal and Skin Diseases, National Institutes of Health (F32AR061923) for fellowship funding to C.M.K. This work was made possible by financial support from the National Institutes of Health (R01 HL089260) and the Howard Hughes Medical Institute.

Received: July 17, 2013
Revised: September 26, 2013
Published online: January 24, 2014

[1] R. J. McMurray, N. Gadegaard, P. M. Tsimbouri, K. V. Burgess, L. E. McNamara, R. Tare, K. Murawski, E. Kingham, R. O. C. Oreffo, M. J. Dalby, *Nat. Mater.* **2011**, *10*, 637.
[2] A. J. Engler, S. Sen, H. L. Sweeney, D. E. Discher, *Cell* **2006**, *126*, 677.
[3] A. Khademhosseini, N. A. Peppas, *Adv. Healthcare Mater.* **2013**, *2*, 10.
[4] C. M. Kirschner, K. S. Anseth, *Acta Mater.* **2013**, *61*, 931.
[5] B. V. Slaughter, S. S. Khurshid, O. Z. Fisher, A. Khademhosseini, N. A. Peppas, *Adv. Mater.* **2009**, *21*, 3307.
[6] C. A. DeForest, K. S. Anseth, *Annu. Rev. Chem. Biomol. Eng.* **2012**, *3*, 421.
[7] A. M. Kloxin, A. M. Kasko, C. N. Salinas, K. Anseth, *Science* **2009**, *234*, 59.
[8] M. Guvendiren, J. A. Burdick, *Adv. Healthcare Mater.* **2012**, *2*, 155.
[9] C. A. DeForest, K. S. Anseth, *Nat. Chem.* **2011**, *3*, 925.
[10] J. C. Culver, J. C. Hoffmann, R. A. Poché, J. H. Slater, J. L. West, M. E. Dickinson, *Adv. Mater.* **2012**, *24*, 2344.
[11] D. R. Griffin, A. M. Kasko, *ACS Macro Lett.* **2012**, *1*, 1330.
[12] S. Sugiura, K. Sumaru, K. Ohi, K. Hiroki, T. Takagi, T. Kanamori, *Sens. Actuators A: Phys.* **2007**, *140*, 176.
[13] D. S. VanBlarcom, N. A. Peppas, *Biomed. Microdevices* **2011**, *13*, 829.
[14] C. M. Kirschner, K. S. Anseth, *Small* **2013**, *9*, 578.
[15] H. Wang, S. M. Haeger, A. M. Kloxin, L. A. Leinwand, K. S. Anseth, *PLoS One* **2012**, *7*, e39969.
[16] A. M. Kloxin, J. A. Benton, K. S. Anseth, *Biomaterials* **2010**, *31*, 1.
[17] J. J. Tomasek, G. Gabbiani, B. Hinz, C. Chaponnier, R. A. Brown, *Nat. Rev. Mol. Cell Biol.* **2002**, *3*, 349.
[18] B. Hinz, *J. Invest. Dermatol.* **2007**, *127*, 526.
[19] C. Li, S. Xu, A. I. Gotlieb, *Cardiovasc. Pathol.* **2013**, *22*, 1.
[20] G. A. Walker, K. S. Masters, D. N. Shah, K. S. Anseth, L. A. Leinwand, *Circ. Res.* **2004**, *95*, 253.
[21] A. H. Chester, P. M. Taylor, *Philos. Trans. R. Soc. Lond B: Biol. Sci.* **2007**, *362*, 1437.
[22] P. M. Taylor, P. Batten, N. J. Brand, P. S. Thomas, M. H. Yacoub, *Int. J. Biochem. Cell Biol.* **2003**, *35*, 113.
[23] D. A. Filip, A. Radu, M. Simionescu, *Circ. Res.* **1986**, *59*, 310.
[24] B. Hinz, G. Gabbiani, *Curr. Opin. Biotechnol.* **2003**, *14*, 538.
[25] W. David Merryman, H.-Y. Shadow Huang, F. J. Schoen, M. S. Sacks, *J. Biomech.* **2006**, *39*, 88.
[26] E. R. Mohler, F. Gannon, C. Reynolds, R. Zimmerman, M. G. Keane, F. S. Kaplan, *Circulation* **2001**, *103*, 1522.
[27] C. Y. Y. Yip, C. A. Simmons, *Cardiovasc. Pathol.* **2011**, *20*, 177.
[28] C. Huang, X. Fu, J. Liu, Y. Qi, S. Li, H. Wang, *Biomaterials* **2012**, *33*, 1791.
[29] K. E. Myrna, R. Mendonsa, P. Russell, S. A. Pot, S. J. Liliensiek, J. V. Jester, P. F. Nealey, D. Brown, C. J. Murphy, *Invest. Ophthalmol. Vis. Sci.* **2012**, *53*, 811.
[30] K. D. Costa, E. J. Lee, J. W. Holmes, *Tissue Eng.* **2003**, *9*, 567.
[31] C. P. Ng, B. Hinz, M. A. Swartz, *J. Cell Sci.* **2005**, *118*, 4731.
[32] P. Ayala, T. A. Desai, *Integr. Biol.* **2011**, *3*, 733.
[33] R. F. Ankeny, V. H. Thourani, D. Weiss, J. D. Vega, W. R. Taylor, R. M. Nerem, H. Jo, *PLoS One* **2011**, *6*, 1.
[34] H.-Y. S. Huang, J. Liao, M. S. Sacks, *J. Biomech. Eng.* **2007**, *129*, 880.
[35] K. A. Kilian, B. Bugarija, B. T. Lahn, M. Mrksich, *PNAS* **2010**, *107*, 4872.
[36] B. D. Polizzotti, B. D. Fairbanks, K. S. Anseth, *Biomacromolecules* **2008**, *9*, 1084.
[37] M. Malkoch, R. Vestberg, N. Gupta, L. Mespouille, P. Dubois, A. F. Mason, J. L. Hedrick, Q. Liao, C. W. Frank, K. Kingsbury, C. J. Hawker, *Chem. Commun.* **2006**, *0*, 2774.
[38] S. T. Gould, N. J. Darling, K. S. Anseth, *Acta Biomater.* **2012**, *8*, 3201.
[39] D. L. Hern, J. A. Hubbell, *J. Biomed. Mater. Res.* **1998**, *39*, 266.
[40] X. Gu, K. S. Masters, *J. Biomed. Mater. Res. Part A* **2010**, *93A*, 1620.
[41] M. W. Tibbitt, A. M. Kloxin, L. A. Sawicki, K. S. Anseth, *Macromolecules* **2013**, *46*, 2785.
[42] D. R. Griffin, A. M. Kasko, *J. Am. Chem. Soc.* **2012**, *134*, 13103.
[43] C. A. DeForest, K. S. Anseth, *Angew. Chem Int. Ed.* **2012**, *51*, 1978.
[44] M. W. Tibbitt, A. M. Kloxin, K. S. Anseth, *J. Polym. Sci., Part A: Polym. Chem.* **2013**, *46*, 2785.
[45] M. van Dijk, C. F. van Nostrum, W. E. Hennink, D. T. S. Rijkers, R. M. J. Liskamp, *Biomacromolecules* **2010**, *11*, 1608.
[46] C. A. DeForest, E. A. Sims, K. S. Anseth, *Chem. Mat.* **2010**, *22*, 4783.
[47] C. M. Johnson, M. N. Hanson, S. C. Helgeson, *J. Mol. Cell. Cardiol.* **1987**, *19*, 1185.